Comparative Analysis of Multilevel-High-Frequency-Link and Multilevel-DC-Link DC–DC Transformers Based on MMC and Dual-Active Bridge for MVDC Application

Biao Zhao, *Member, IEEE*, Qiang Song, *Member, IEEE*, Jianguo Li, Xiaopeng Xu, and Wenhua Liu

***Abstract*—This paper gives a comprehensive comparison of multilevel high-frequency-link (HFL) dc transformer (abbreviated MDCT) based on modular multilevel converter (MMC) and multilevel-dc-link dc transformer (abbreviated ADCT) based on dual-active-bridge (DAB) for medium-voltage dc (MVDC) application. The topology, operation, HFL voltage and current, active and circulating power, characteristic currents, switching behaviors, and power loss are analyzed in detail. Both MDCT and ADCT have fault treatment ability for MVDC application. However, the installation and commissioning of ADCT are more flexible and simpler. In addition, the MDCT needs more switches and high-frequency (HF) inductors than ADCT in the MVDC side with the same voltage level, but the number of HF transformer can be reduced. Compared with MDCT, the ADCT has higher power transfer ability and lower circulating power, lower HFL voltage, and RMS current and peak values with the same transmission power in the MVDC side. However, the arm RMS and average currents of MDCT are lower than those of ADCT in the MVDC side. The switching performance of MDCT deteriorates when the MVDC voltage fluctuates, but the switching behaviors of half bridges are added to ADCT. The loss of ADCT almost keep the same when the MVDC voltage fluctuates, but the loss of MDCT changes a lot. Finally, a small-scale prototype platform with 1 kW/450 V/150 V is built and experimental results verify the correctness and effectiveness of the theoretical analysis.**

***Index Terms*—dc distribution, dc transformer, Dual-active bridge (DAB), high-frequency link (HFL), high-voltage dc (HVDC), medium-voltage dc (MVDC), modular multilevel converter (MMC), solid-state transformer.**

Manuscript received December 5, 2016; revised February 20, 2017; accepted April 19, 2017. Date of publication May 2, 2017; date of current version December 1, 2017. This work was supported by the National Key R&D Program of China under Grant 2016YFB0901002. Recommended for publication by Associate Editor Drazen Dujic. *(Corresponding Author: Qiang Song.)*

B. Zhao, Q. Song, and W. Liu are with the Department of Electrical Engineering, Tsinghua University, Beijing 100084, China (e-mail: zhaobiao112904829@126.com; songqiang@tsinghua.edu.cn; liuwenh@tsinghua.edu.cn).

J. Li is with the Department of Electrical Engineering, Tsinghua University, Beijing 100084, China (e-mail: lijianguo@tsinghua.edu.cn).

X. Xu is with the Liaoning Electric Power Company Limited, Shenyang 110000, China (e-mail: xxp_ln@163.com).

Color versions of one or more of the figures in this paper are available online at http://ieeexplore.ieee.org.

Digital Object Identifier 10.1109/TPEL.2017.2700378

I. Introduction

MEDIUM-VOLTAGE dc (MVDC) distribution grid is a key link to build modern dc grid [1]–[3], especially as an intermediate link to connect high-voltage dc (HVDC) transmission grid and low-voltage dc (LVDC) microgrid [4], [5]. In this case, dc–dc transformer (DCT) is a key component to directly achieve dc power conversion and transfer [6]. The DCT may exist for different links in future dc grid. This paper mainly focuses on the DCT scheme between MVDC and LVDC systems. In fact, compared to HVDC system, the MVDC system will have more flexibility. In particular, considering integration of renewable energy and power supply security, unidirectional power transfer [7] and nonisolation [8] schemes cannot satisfy the requirements of future MVDC system, the DCT should be designed as a bidirectional system with electrical isolation. Different with ac magnetic transformer, which is easily achieved in ac grid, achieving DCT in MVDC application is difficult [9]. A common solution is to achieve high-frequency (HF) ac link by power electronic converters and then to achieve electrical isolation by ac magnetic transformer [10]. In fact, in LVDC application, isolated bidirectional dc–dc converter has been widely researched. A typical topology is dual-active-bridge (DAB) dc–dc converter [11], which has bidirectional power transfer capacity and fast dynamic response [12]. In addition, DAB has good soft-switching performances and can achieve high efficiency even operating at high switching frequency [13], so the power density is high, and it is commonly considered as a core circuit for next-generation high-density power conversion system [14].

However, because of the limitation of power electronic switches, accessing MVDC grid is hard for a single DAB. Based on the standard single-phase full-bridge DAB, three-phase DAB is proposed to increase power capacity and power density [15]; three-level neutral-point-clamped (NPC) DAB [16] and T-type DAB [17], [18] schemes are also proposed to improve high-frequency-link (HFL) performances and voltage level. However, these schemes still cannot reach the requirements of voltage level, power capacity of MVDC application. To further increase the voltage level of DAB, switch-series scheme is also

discussed [19]; however, balance operation of series switches in HF states is a technical bottleneck, and normally, open devices are employed. Based on these studies, a typical solution for MVDC application is the input-series output-parallel (ISOP) topology [20]–[23], which has been widely studied and applied in literatures because of good modularity and simple operation. The series connection can increase the voltage level, whereas the parallel connection can increase the power level. However, if we put this kind of DCT into MVDC grid, then a large overcurrent will be produced because of concentrated dc capacitor when a short-circuit fault occurs in MVDC grid. Thus, an additional dc breaker should be added. In addition, because of the power/voltage limitation of semiconductor switches, dozens of DAB cells are needed in MVDC application. If a DAB cell breaks down in operation, it is possible for DCT to bypass a fault DAB because there is a concentrated dc capacitor for each DAB in series side; otherwise, the dc capacitor will be short-circuited. Therefore, the system will stop operating even if just a DAB cell breaks down. Thus, the reliability of the system will be decreased without redundant unit. Moreover, for DAB, both the primary and secondary voltages of the transformer in HFL are two-level square waves. A large circulating current is produced when the terminal voltages do not match the turn ratio of the transformer. Then, the current impact will be high and the efficiency will be low.

To solve the problems stated earlier, the current research tends to employ modular multilevel converter (MMC) into DCT [20]–[29]. Especially, a multilevel and multiplex HFL DCT topology based on MMC (abbreviated as MDCT in this paper, where "M" represents the MMC-based system) was proposed to connect MVDC and LVDC buses [29]. In fact, the control of MMC may be difficult or unprocurable in HVDC applications because of hundreds of series submodules (SMs). However, in MVDC, the voltage is just several kilovolts, the number of SMs is just dozens, which decreases the control difficulty. In [30], an improved DAB-based DCT topology (abbreviated as ADCT in this paper, where "A" represents DAB-based system) based on switched capacitor was also proposed. In fact, ADCT can also be seen that an MMC arm is added in the MVDC side, and the multilevel modulation can be used in the dc side. Although the losses of the added MMC arm may decrease the efficiency of ADCT during matching state, the efficiency of ADCT is still higher than standard ISOP topology during mismatching state because the MMC arm can make DAB in ADCT always operate with a matching state [30].

In both MDCT and ADCT topologies, MMC structure changes concentrated capacitor into discrete capacitors, which can operate as a dc breaker and enhance the reliability and flexibility of the system. However, they have different solution thinking. MDCT employs a whole MMC as an MVDC interface, and then the HFL can be operated with multilevel modulation. ADCT is still to employ DAB as a basic cell and just employs an MMC arm as an MVDC interface, and then the dc link can be operated with multilevel modulation. Thus, the operation and performances have similar aspects and many differences. This paper gives a comprehensive comparison of MDCT and ADCT to make a clear understanding on how to effectively operate DCT based on MMC and DAB in MVDC application.

TABLE I
TECHNICAL CHARACTERISTICS OF MDCT AND ADCT

Item	MDCT	ADCT
Switch	$8*n$ for MVDC $4*m$ for LVDC	$6*n$ for LVDC $4*n$ for LVDC
Transformer	m HF transformers	n HF transformers
Power density	Low density in the MVDC side High density in the LVDC side	High density in the MVDC side Low density in the LVDC side.
Reliability	Treatment ability for short-circuit fault and redundancy	Treatment ability for short-circuit fault and redundancy
Control implementation	Concentrated control for a whole system	Distributed control for each extended DAB
Installation and commissioning	With a whole MMC	With an extended DAB

The paper is organized as follows. Section II analyzes the topologies of MDCT and ADCT and compares the technical characteristics. Section III gives a comprehensive comparison of HFL operation, especially the dual-active phase-shift principle, HFL voltage and current, transmission power, and circulating power performances. Section IV compares the characteristic currents of MDCT and ADCT with the same transmission power. On this basis, Section V gives a comparison of switching performances. In Section VI, power loss is also analyzed. Section VII gives a comprehensive experimental verification.

II. TOPOLOGY COMPARISON

The topologies of MDCT and ADCT are shown in Fig. 1. MDCT employs an MMC structure to increase the voltage level. Each bridge arm is composed of n SMs and an HF inductor. The HFL is composed of m HF isolated transformers, which are connected in series in the primary side. The LVDC interface of MDCT is composed of m full bridges, which are connected in parallel in dc side to increase the current level. ADCT still employs DAB structure as a basic cell. The system is composed of n DAB modules, but the series multilevel dc link (MDCL) based on half-bridge SM is used as the interface for MVDC. The comparison of the basic technical characteristics of MDCT and ADCT are shown in Table I. By using the SM, no concentrated capacitor was produced in the MVDC side for both MDCT and ADCT. The redundant module can be added easily in both DCTs, and then the DCTs can operate well when some SMs fail. Moreover, when a short-circuit fault is produced in the MVDC grid, the DCTs can work as a dc breaker to cut off the connection between MVDC and LVDC buses. According to the earlier analysis, both MDCT and ADCT have treatment ability for short-circuit fault and redundancy in MVDC application. With the same voltage level, MDCT and ADCT, respectively, need $8*n$ and $6*n$ switches for the MVDC side that means MDCT also needs more driving and control auxiliary circuits. In addition, MDCT needs $4*n$ discrete dc capacitors but ADCT just needs n discrete capacitor in the MVDC side, and MDCT needs four-arm HF inductors but ADCT does not need four-arm HF inductors. Although the switches in MMC of MDCT can have smaller rated current, but the increased volume will not that much compared with the more switches, capacitors, inductors, and auxiliary circuits. Therefore, ADCT has higher

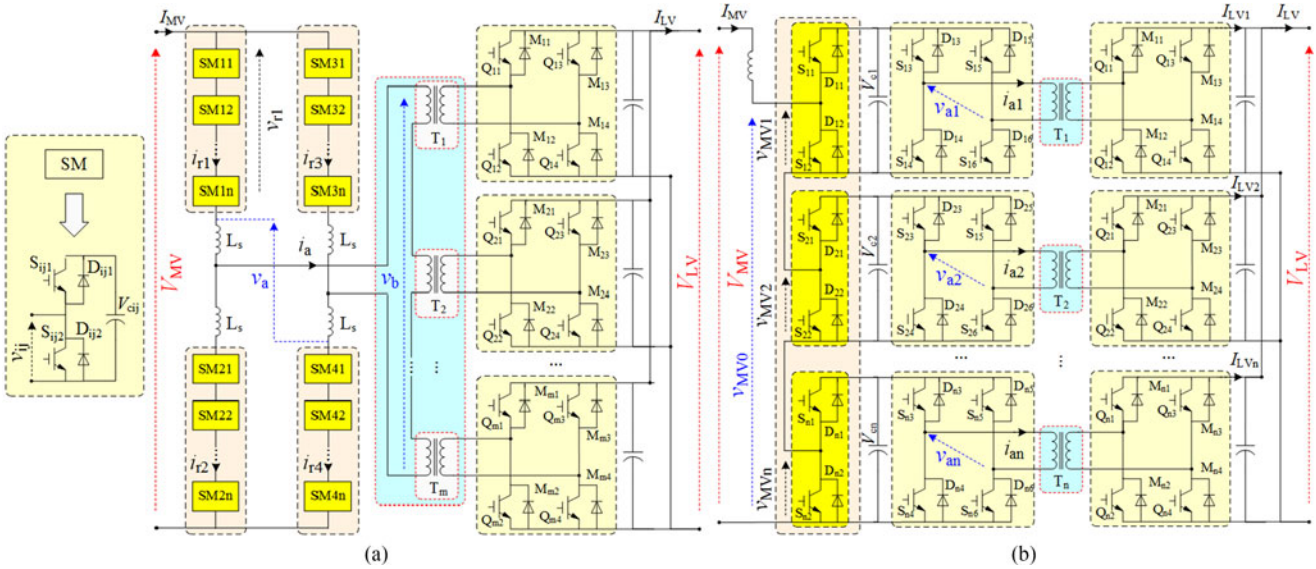

Fig. 1. Comparison of topology for (a) MDCT and (b) ADCT.

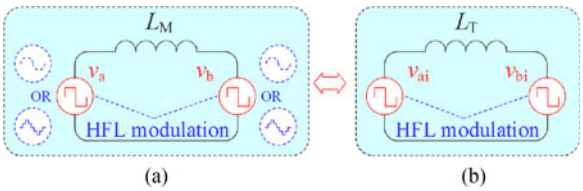

Fig. 2. Dual-active phase-shift principle for (a) MDCT and (b) ADCT.

power density in the MVDC side. In the LVDC side, the number of H-bridges for MDCT in the LVDC side is just decided by the power and can be fewer than the number of SMs in the MVDC side. Thus, *m* can be fewer than *n*, but the number of H-bridges for ADCT should be equal to *n*. Therefore, the number of switches in MDCT can be fewer than that in ADCT in the LVDC side. In this case, with the same rated power, the number of HF transformers in MDCT also can be fewer than that in ADCT. Therefore, MDCT has higher power density in the LVDC side.

In fact, in practice, the transformers in MDCT are connected in series and in ADCT are distributed to each DAB, that just cause the operation voltages of primary and secondary sides of transformer are not high. However, in order to satisfy the isolation of the MVDC system, the isolation voltage between primary and secondary sides of each transformer needs to be high, which increases the manufacturing difficulty and the volume of HF transformer greatly. Therefore, reducing the number of HF transformer in a certain degree is welcome in practice.

In addition, although MDCT employs modular structure in topology, it still needs concentrated control system to modulate all the SMs in an MMC, especially because the number of SMs is high and all the SMs operate in HF states in MVDC application, the control complexity is increased. In ADCT, each SM of the MMC leg can be seen as a separate buck/boost converter; then one SM and one DAB can be seen as a two-stage dc–dc cell, and the balance control of the MMC leg can also be embedded to the corresponding DAB cell, so the control of ADCT has more modularity. Moreover, the MDCT just can operate with a whole system, but every cell of ADCT can operate not only independently but also in series to connect the MVDC bus, which decreases the difficulty of installation and commissioning in practice.

III. Operation Characterization Comparison

A. Dual-Active Phase-Shift Operation

Both MDCT and ADCT employ dual-active phase-shift principle to transfer power, as shown in Fig. 2. For MDCT, the whole system is equivalent to two HF waves v_a and v_b connected with an inductor. For ADCT, each cell is equivalent to two HF waves v_{ai} and v_{bi} connected with an inductor. Then, for both DCTs, the magnitude and direction of power flow can be adjusted by controlling the magnitude and direction of phase-shift angle between two HF waves.

In HFL modulation, the ADCT can just employ square modulation, whereas the MDCT can employ not only square modulation but also multilevel modulation, such as triangular, sine, and trapezoid modulations. However, according to the analysis in previous literatures, the square modulation has higher power transfer ability, better current performance, and simpler control method. Therefore, the square modulation will be employed for MDCT to compare with the performance of ADCT in this paper. In practice, to decrease the voltage stress of square modulation, there will be a phase-shift angle between neighboring SMs. However, because the phase-shift angle is very small, the performance can be approximated with the ideal square modulation to simplify the theoretical analysis [24]. In Fig. 2, L_T is equivalent HFL inductance of each DAB cell, and L_M is equivalent HFL inductance of the whole MDCT. In this paper, assuming that both DCTs have the same HFL inductances L, we have

$$L = nL_T = L_M. \tag{1}$$

B. Balance Control

Voltage balance of dc capacitors in MMC and current balance in H-bridges are the key for the stable operation of MDCT. Because the transformers are connected in series in the primary side and the turn ratio of the transformer are the same, so the current flows to H-bridges are balanced automatically. As for the MMC part, because there is a phase shift between different SMs, although the currents in the same position of different arms are the same, the capacitor currents for different SMs in the same arm are also different. To ensure the voltage balance of MMC capacitors, the alternate modulation should be employed, as shown in Fig. 3(a). The output of every SM is not constant but changes alternately. However, the output voltage of the whole arm remains the same. In this case, the average current of the dc capacitor during an alternate period will be the same. In addition, to adjust the unbalance caused by inconsistency of hardware and software, an additional control link is also needed. The arm current's direction is measured every moment, and the SM controller will delay the rising or falling edge of the pulse received according to the direction of the arm current and the error of voltage between the SM voltage and the average voltage, to adjust the capacitor voltage.

For ADCT, the voltage balance of discrete capacitors in SMs and the current balance in the LVDC side are the key for the stable operation. From [30], if the voltage balance of discrete capacitors is controlled, the current balance in the LVDC side will be achieved automatically. The voltage balance for ADCT can be achieved by SMs and DABs. In order to avoid centralized control, the balance control can be distributed to each DAB cell, as shown in Fig. 3(b). There is also an additional balance controller for each DAB. However, the alternate balance is not needed, each DAB can achieve balance control by itself.

According to the earlier analysis, each SM in MDCT will need an additional balance controller and the alternate modulation for each arm should be provided. Each DAB in ADCT will need an additional balance controller and the alternate modulation is not needed. From Section II, with the same voltage level, there are 4*n* SMs in MDCT and *n* DABs in ADCT, so the calculation of balance control for MDCT will be more complex than that of ADCT.

In Fig. 3, β is the phase-shift angle for the whole MDCT to adjust the power flow and β_i is the phase-shift angle for each DAB in ADCT; V_{cij} and V_{ci} are the voltages of discrete dc capacitor in MDCT and ADCT, respectively; $V_{ciaver} = (V_{ci1} + V_{ci2} \ldots + V_{cin})/n$ are the average voltage of dc capacitors for each arm in MDCT, and $V_{\mathrm{caver}} = (V_{c1} + V_{c2} + \ldots + V_{cn})/n$ are the average voltage of discrete capacitors in ADCT; i_{ri} is the arm current in MMC of MDCT; and $I_{\mathrm{LV}i}$ is the dc current for each DAB in the LVDC side.

IV. HFL Characterization Comparison

A. HFL Characterization

For MDCT, the circulating power, current stress, and power loss will increase greatly when the voltages of MVDC grid are not rated voltages. Considering the voltage-adjusting ability of SMs in ADCT, no matter how the voltage of MVDC grid fluctuates, the HFL voltages always match the turn ratio of the transformer. Thus, the current keeps a constant value during the peak point, which decreases the current stress and switching loss. Although the losses of the added MMC arm may decrease the efficiency of ADCT during matching state, the efficiency of ADCT is still higher than the standard ISOP topology with the same transmission power during most of ranges of mismatching state because the MMC arm can make DAB in ADCT always operate with a matching state. In fact, because the real MVDC system has not been applied widely until now, there is no common standard or requirement for MVDC voltage fluctuations. However, because there are a lot of power electronics systems to help adjusting voltage in MVDC grid, so the voltage fluctuation requirements of a grid bus can be not that strict as an ac gird.

Assuming that all the voltages of dc capacitors are balanced, *D* is the duty ratio of MDCL in ADCT, which represents the voltage-adjusting ability of SMs. In practice, we have

$$V_{cN\_A} = \frac{V_{\mathrm{MV}}}{n(1-D)} \tag{2}$$

where V_{cN_A} is the rated voltage of dc capacitors in ADCT.

To ensure voltage matching, *D* will be controlled according to the change of MVDC voltage V_{MV} to ensure that V_{cN_A} is constant. From (2), the MMC stage for ADCT is a boost converter, the controller just can adjust dc capacitor voltage to be higher than MVDC voltage. To make sure that the system can still keep match when MVDC voltage reaches the maximum value, the rated voltages of dc capacitors are defined based on the maximum MVDC operation voltage in practice, that is

$$V_{cN\_A} = \frac{(1+\lambda_{\max})V_{\mathrm{MVN}}}{n} \tag{3}$$

where $\lambda_{\max}$ is the maximum fluctuation rate of MVDC grid and V_{MVN} is the rated voltage of MVDC grid.

The allowable fluctuation rate of MVDC voltage is assumed as 5% in this paper, that is, $\lambda_{\max} = 5\%$. Thus, to ensure voltage matching, the turn ratio of the HF transformer is designed based on the rated voltage of dc capacitors (the maximum MVDC voltage) for ADCT, that is, $n_{T_A} = V_{cN_A}/V_{\mathrm{LV}} = (1+\lambda_{\max})V_{\mathrm{MVN}}/(nV_{\mathrm{LV}})$. As for MDCT, the turn ratio of the HF transformer is designed based on the rated MVDC voltage and the series number of transformer, that is, $n_{T\_M} = V_{\mathrm{MVN}}/(mV_{\mathrm{LV}})$. From [29] and [30], the HFL voltage and the current and power of MDCT and ADCT are shown in Table II, where A_1, B_1, A_2, and B_2 are the rated coefficients as follows:

$$\begin{cases} A_1 = V_{\mathrm{MVN}}\cos(k\beta_M) - V_{\mathrm{MV}} \\ B_1 = V_{\mathrm{MVN}}\sin(k\beta_M) \\ A_2 = (1+\lambda_{\max})V_{\mathrm{MVN}}[\cos(k\beta_A) - 1] \\ B_2 = (1+\lambda_{\max})V_{\mathrm{MVN}}\sin(k\beta_A) \end{cases}. \tag{4}$$

B. HFL Voltage and Current Performance

Fig. 4 shows the HFL voltage and the current performance for MDCT and ADCT. As shown in the figure, the HFL voltage

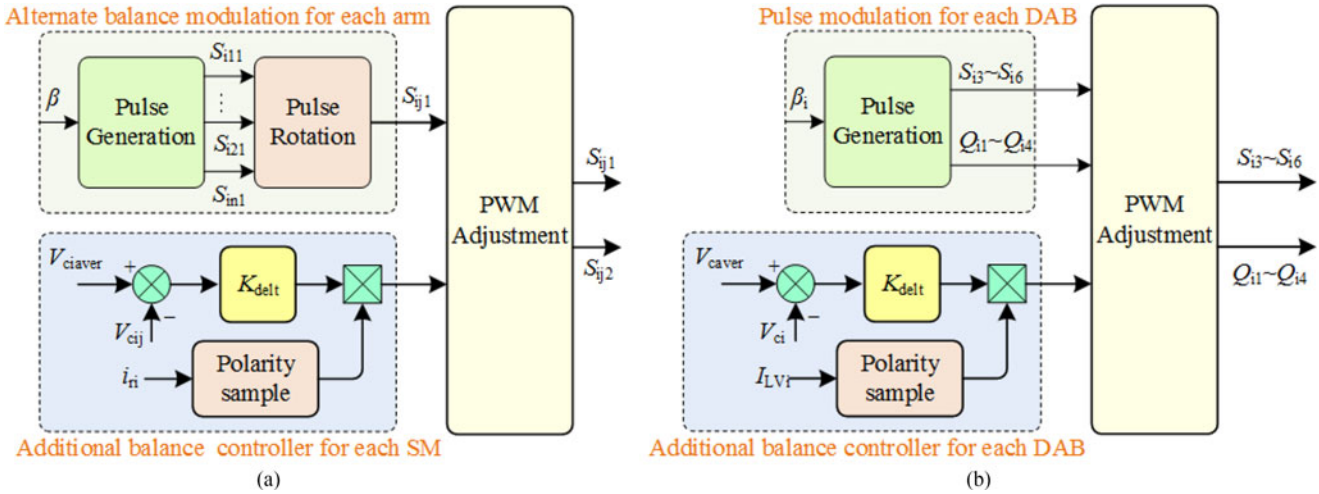

Fig. 3. Balance control for (a) MDCT and (b) ADCT.

TABLE II
HFL VOLTAGE, CURRENT, AND POWER OF MDCT AND ADCT

Variable	MDCT	ADCT
HFL voltage in MV side	$v_a = \sum_{k=1,3,5,\ldots} \frac{4V_{\mathrm{MV}}}{k\pi}\sin(kw_0t)$	$v_{ai} = \sum_{k=1,3,5,\ldots} \frac{4V_{\mathrm{MV}}}{kn\pi(1-D)}\sin(kw_0t)$
HFL voltage in LV side	$v_b = \sum_{k=1,3,5,\ldots} \frac{4V_{\mathrm{MVN}}}{k\pi}\sin k(w_0t-\beta_M)$	$v_{bi} = \sum_{k=1,3,5,\ldots} \frac{4V_{\mathrm{MV}}}{kn\pi(1-D)}\sin[k(w_0t-\beta_A)]$
HFL current	$i_a = \sum_{k=1,3,5,\ldots} \frac{4\sqrt{{A_1}^2+{B_1}^2}}{k^2\pi w_0 L}\sin(kw_0t+\arctan\frac{A_1}{B_1})$	$i_{ai} = \sum_{k=1,3,5,\ldots} \frac{4\sqrt{{A_2}^2+{B_2}^2}}{k^2\pi w_0 L}\sin(kw_0t+\arctan\frac{A_2}{B_2})$
Transmission power	$P_M = \sum_{k=1,3,5,\ldots} \frac{8V_{\mathrm{MV}}V_{\mathrm{MVN}}}{k^3\pi^2 w_0 L}\sin(k\beta_M)$	$P_A = \sum_{k=1,3,5,\ldots} \frac{8V_{\mathrm{MV}}V_{\mathrm{MVN}}(1+\lambda_{\max})}{k^3\pi^2 w_0 L(1-D)}\sin(k\beta_A)$

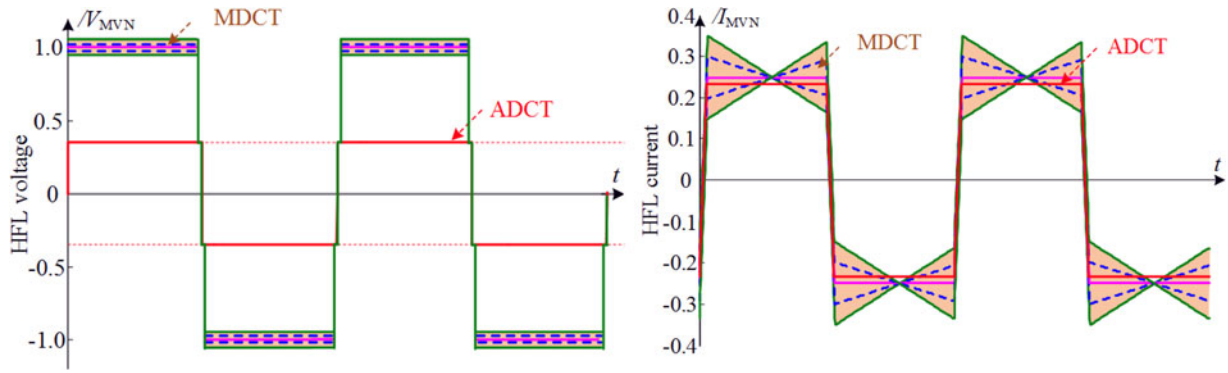

Fig. 4. Comparison of HFL voltage and current for MDCT and ADCT: (a) HFL voltage and (b) HFL current.

and current of MDCT will change with the voltage fluctuation of the MVDC grid, but the HFL voltage and current of ADCT always remain the same. As a result of the square modulation of MDCT, the maximum value of HFL voltage in ADCT is just $1/n$ times of V_{MV}, which is lower than that of MDCT. In addition, no matter how the MVDC voltage changes, the HFL current in ADCT is lower than that of MDCT with the same transmission. The detailed analysis of current rating will be introduced in Section IV. In Fig. 4, the LVDC voltage is controlled by DCT with rated voltage; V_{MV} changes with maximum fluctuation rate 5%; HFL voltage and current are normalized by V_{MVN} and I_{MVN} in Section IV; and the number of SMs is $n = 3$.

C. HFL Transmission Power Performance

Assuming the stray inductances of the systems hold, the transmission power performance is shown in Fig. 5(a). It can be seen that the transmission power achieves the maximum value when the phase-shift angle is $\pi/2$ both for MDCT and ADCT. The transmission ability is greater than that of MDCT because of the voltage-adjusting ability of SMs in ADCT. In fact, the

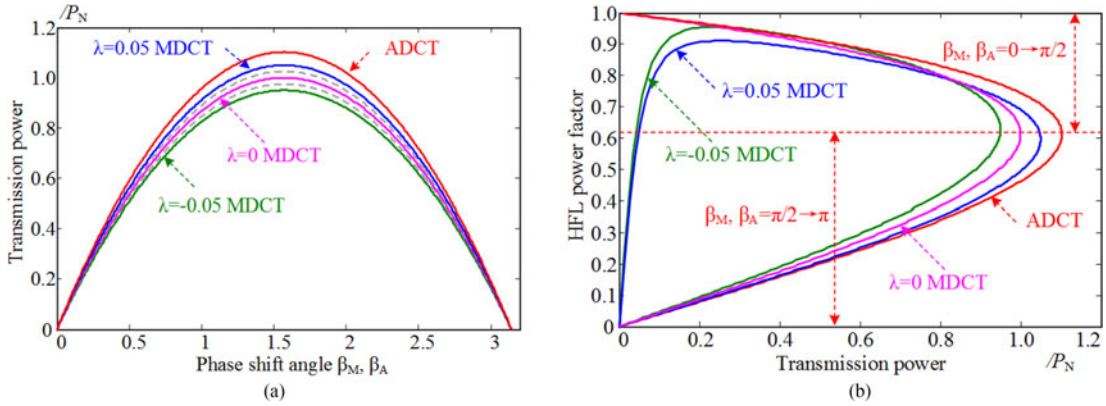

Fig. 5. Comparison of power performance for MDCT and ADCT. (a) Transmission power. (b) Circulating power.

power transmission ability of ADCT can be further increased if the voltage of the dc capacitor is adjusted higher than that of the rated voltage. According to the earlier analysis, ADCT can always get higher power ability than MDCT. In Fig. 5, the power is normalized as

$$P_N = \frac{V_{\mathrm{MVN}} V_{\mathrm{MVN}}}{8 f_s L}. \tag{5}$$

D. HFL Circulating Power Performance

For DCT, the circulating power can be described by HFL power factor, that is

$$\begin{cases} \gamma_M = \dfrac{P_M}{S_M} = \dfrac{P_M}{V_a I_a} \\ \gamma_A = \dfrac{P_A}{S_A} = \dfrac{P_A}{n V_{ai} I_{ai}} \end{cases} \tag{6}$$

where V_a, I_a, V_{ai}, and I_{ai} are the HFL voltage and RMS current of MDCT and ADCT, respectively.

Then, the curves of HFL power factor varied with transmission power is shown in Fig. 5. No matter how the MVDC voltage fluctuates, the ADCT always has a higher power factor (that is lower circulating power) than MDCT with the same transmission power. In addition, the power factor when $\pi/2 \le \beta_M, \beta_A \le \pi$ is lower than that when $\pi/2 \ge \beta_M, \beta_A \ge 0$, because the transmission power characterization is the same, so the phase-shift angle just need to be designed during [0, π/2] in practice. In fact, there are also some advanced modulations, which are proposed to suppress the circulating current in traditional DAB [10], such as dual phase shift, extended phase shift, triple phase shift, etc. These methods are also can be employed to MMC in MDCT; however, no matter which advanced modulation is used, it just can suppress the circulating current in a certain degree, and the circulating current of MDCT will be still higher than that of ADCT because the dc voltage of each capacitor in MMC is still a constant.

According to the earlier analysis, compared with MDCT, ADCT has lower HFL voltage and current peak, higher power transfer ability, and lower circulating power.

V. Characteristic Current Comparison

A. Characteristic Current Comparison in MVDC Side

From Table II, the HFL RMS current I_a of MDCT can be derived based on the RMS value of each component in Fourier series

$$I_a = \frac{4}{\pi w_0 L} \sqrt{\sum\nolimits_{k=1,3,5,\ldots} \frac{{A_1}^2 + {B_1}^2}{2k^4}}. \tag{7}$$

For MMC in MDCT, the arm current is composed of the MVDC current and the HFL current; so we have

$$\begin{cases} I_{r\_M} = \sqrt{\left(\dfrac{I_{\mathrm{MV}}}{2}\right)^2 + \left(\dfrac{I_a}{2}\right)^2} = \sqrt{\left(\dfrac{P_M}{2V_{\mathrm{MV}}}\right)^2 + \left(\dfrac{I_a}{2}\right)^2} \\ \hat{I}_{r\_M} = \dfrac{1}{T}\displaystyle\int_0^T \left|\frac{I_{\mathrm{MV}}}{2} + \frac{i_a}{2}\right| dt = \frac{1}{T}\int_0^T \left|\frac{P_M}{2V_{\mathrm{MV}}} + \frac{i_a}{2}\right| dt \end{cases} \tag{8}$$

where I_{r_M} and $\hat{I}_{r_M}$ are the arm RMS current and the arm absolute average current of MDCT, respectively.

From Fig. 4, when $V_{\mathrm{MV}} < n_{T_M} m V_{\mathrm{LV}}$, the current stress for MMC in MDCT will be achieved for the HFL current at $\omega_0 t = \beta_M$; when $V_{\mathrm{MV}} \ge n_{T_M} m V_{\mathrm{LV}}$, current stress will be achieved for the HFL current at $\omega_0 t = \pi$. From Table II and (4), we have

$$I_{m\_M} = \begin{cases} \dfrac{P_M}{2V_{\mathrm{MV}}} + \displaystyle\sum_{k=1,3,5,\ldots} \frac{2[V_{\mathrm{MVN}} - V_{\mathrm{MV}}\cos(k\beta_M)]}{k^2 \pi w_0 L} & w_0 t = \beta_M \\ \dfrac{P_M}{2V_{\mathrm{MV}}} + \displaystyle\sum_{k=1,3,5,\ldots} \frac{2[V_{\mathrm{MV}} - V_{\mathrm{MVN}}\cos(k\beta_M)]}{k^2 \pi w_0 L} & w_0 t = \pi \end{cases}. \tag{9}$$

Similar to ADCT, for DAB cell, the arm RMS current can be described with HFL RMS current; for SMs, the arm RMS current can be described with MVDC RMS current. In addition, for DAB cells in ADCT, the current stress will be achieved for HFL current at $\omega_0 t = \beta_A$ or $\omega_0 t = \pi$. In fact, for DAB cells in ADCT, the currents for $\omega_0 t = \beta$ and $\omega_0 t = \pi$ are the same during the matching state. For SMs in ADCT, if ignoring the current fluctuation in the MVDC side, the current stress is the same with average current in the MVDC side. Then, the current characterization for MDCT and ADCT is shown in

TABLE III
CURRENT CHARACTERIZATION OF MDCT AND ADCT IN THE MVDC SIDE

Variable	MDCT	ADCT	
		DAB	SM
HFL RMS current	$I_a = \frac{4}{\pi w_0 L}\sqrt{\sum_{k=1,3,5,\ldots}\frac{A_1^2+B_1^2}{2k^4}}$	$I_{ai} = \frac{4}{\pi w_0 L}\sqrt{\sum_{k=1,3,5,\ldots}\frac{A_2^2+B_2^2}{2k^4}}$	
Arm RMS current	$I_{r\_M} = \sqrt{(\frac{P_M}{2V_{MV}})^2+(\frac{I_a}{2})^2}$	$I_{r\_H1} = I_{ai}$	$I_{r\_SM} = \frac{P_A}{V_{MV}}$
Arm absolute average current	$\widehat{I}_{r\_M} = \frac{1}{T}\int_0^T \left\lvert \frac{P_M}{2V_{MV}} + \frac{i_a}{2}\right\rvert dt$	$\widehat{I}_{r\_H1} = \frac{1}{T}\int_0^T \lvert i_{ai}\rvert dt$	$\widehat{I}_{r\_SM} = \frac{P_A}{V_{MV}}$
Current stress	$I_{m\_M} = \frac{P_M}{2V_{MV}} + \sum_{k=1,3,5,\ldots}\frac{2[V_{MVN}-V_{MV}\cos(k\beta_M)]}{k^2\pi w_0 L}$ or $I_{m\_M} = \frac{P_M}{2V_{MV}} + \sum_{k=1,3,5,\ldots}\frac{2[V_{MV}-V_{MVN}\cos(k\beta_M)]}{k^2\pi w_0 L}$	$I_{m\_H1} = \sum_{k=1,3,5,\ldots}\frac{4(1+\lambda_{\max})V_{MVN}[1-\cos(k\beta)]}{k^2\pi w_0 L}$	$I_{m\_SM} = \frac{P_A}{V_{MV}}$

Table III, where I_{ai}, I_{r_H1}, $\hat{I}_{r\_H1}$, and I_{m_H1} are the HFL RMS current, arm RMS current, arm absolute average current, and current stress of H-bridges in the MVDC side in ADCT, respectively; and I_{r_SM}, $\hat{I}_{r\_SM}$, and I_{m_SM} are the arm RMS current, the arm absolute average current, and the current stress of SMs in ADCT, respectively.

According to the earlier analysis, the characteristic current comparison in the MVDC side is shown in Fig. 6. It can be seen that the HFL RMS current of MDCT changes with the change in the MVDC voltage, but the HFL RMS current of ADCT remain the same. No matter how the MVDC voltage fluctuates, MDCT has higher HFL current than ADCT with the same transmission power in the entire the range. Although MDCT has higher HFL RMS current, the MDCT has lower arm current than ADCT with the same transmission power at all ranges, and the SMs in ADCT have lower arm RMS current than the DABs during most of the ranges. Similar to the arm RMS current, MDCT has lower arm average current than ADCT with the same transmission power during most of the range; this may increase the conduction loss of switches. Moreover, the SMs in ADCT also have lower arm average current than DABs during most of the range. MDCT has lower arm current than ADCT, but the current stress is higher than that of ADCT with the same transmission power during most of the range, and the SMs in ADCT have the lowest current stress.

In Fig. 6, $V_{\rm MV}$ changes with maximum fluctuation rate of 5%, and all the currents are normalized by $I_{\rm MVN}$ as

$$I_{\rm MVN} = \frac{P_N}{V_{\rm MVN}} = \frac{V_{\rm MVN}\pi}{4w_0 L}. \tag{10}$$

According to the earlier analysis, with the same transmission power, MDCT has higher HFL current and current stress than that of ADCT during most of the range, but the arm RMS and average currents are lower than those of ADCT. Usually, high HFL RMS current will increase the power requirement and conduction loss of HF transformers and inductors, high arm average and RMS currents will increase the current requirement of employed switches and also increase the conduction loss of switches, and high current stress will increase the switching loss and EMI of the system.

TABLE IV
CURRENT CHARACTERIZATION OF MDCT AND ADCT IN THE LVDC SIDE

Variable	MDCT	ADCT
HFL RMS current	$I_b = n_{T\_M} I_a$	$I_{bi} = n_{T\_A} I_{ai}$
Arm RMS current	$I_{r\_H} = I_b$	$I_{r\_H2} = I_{bi}$
Arm absolute average current	$\widehat{I}_{r\_H} = \frac{1}{T}\int_0^T \lvert i_b\rvert dt$	$\widehat{I}_{r\_H2} = \frac{1}{T}\int_0^T \lvert i_{bi}\rvert dt$
Current stress	$I_{m\_H} = n_{T\_M} I_{m\_M}$	$I_{m\_H2} = n_{T\_A} I_{m\_H1}$

B. Characteristic Current Comparison in the LVDC Side

From the earlier analysis, both the LVDC sides for MDCT and ADCT are H-bridges and the characteristic current in the LVDC side is simpler compare with the characteristic current in the MVDC side. For H-bridges in MDCT, because the transformer is connected in series, all the HFL currents are the same and the HFL RMS current I_b of MDCT is $n_{T_M} I_a$; the arm RMS current can be described with the HFL RMS current; the current stress is also achieved for HFL current at $\omega_0 t = \beta_M$ or $\omega_0 t = \pi$. Similar to the H-bridges in ADCT. Then, the current characterization for MDCT and ADCT in the LVDC side is shown in Table IV, where I_b, I_{r_H}, $\hat{I}_{r_H}$, and I_{m_H} are the HFL RMS current, the arm RMS current, the arm absolute average current, and the current stress of H-bridges in MDCT; I_{bi}, I_{r_H2}, $\hat{I}_{r\_H2}$, and I_{m_H2} are the HFL RMS current, the arm RMS current, the arm absolute average current, and the current stress of H-bridges in the LVDC side in ADCT, respectively.

Although both the LVDC sides for MDCT and ADCT are H-bridges, the number of H-bridges may be different. In ADCT, the number of H-bridges in the LVDC side is equal to that in the MVDC side, i.e., n. In MDCT, because the MVDC and the LVDC sides are decoupled, the number of H-bridges in the LVDC side can be more than, less than, or equal to n, which is decided by the employed switches. Therefore, in the LVDC side, the analysis should contain three different cases when $m < n$, $m = n$, and $m > n$.

Fig. 7 shows the characteristic current comparison of MDCT and ADCT in the LVDC side. When $m < n$, all the characteristic currents of MDCT are higher than that of ADCT. When $m > n$, all the characteristic currents of MDCT are lower than that of

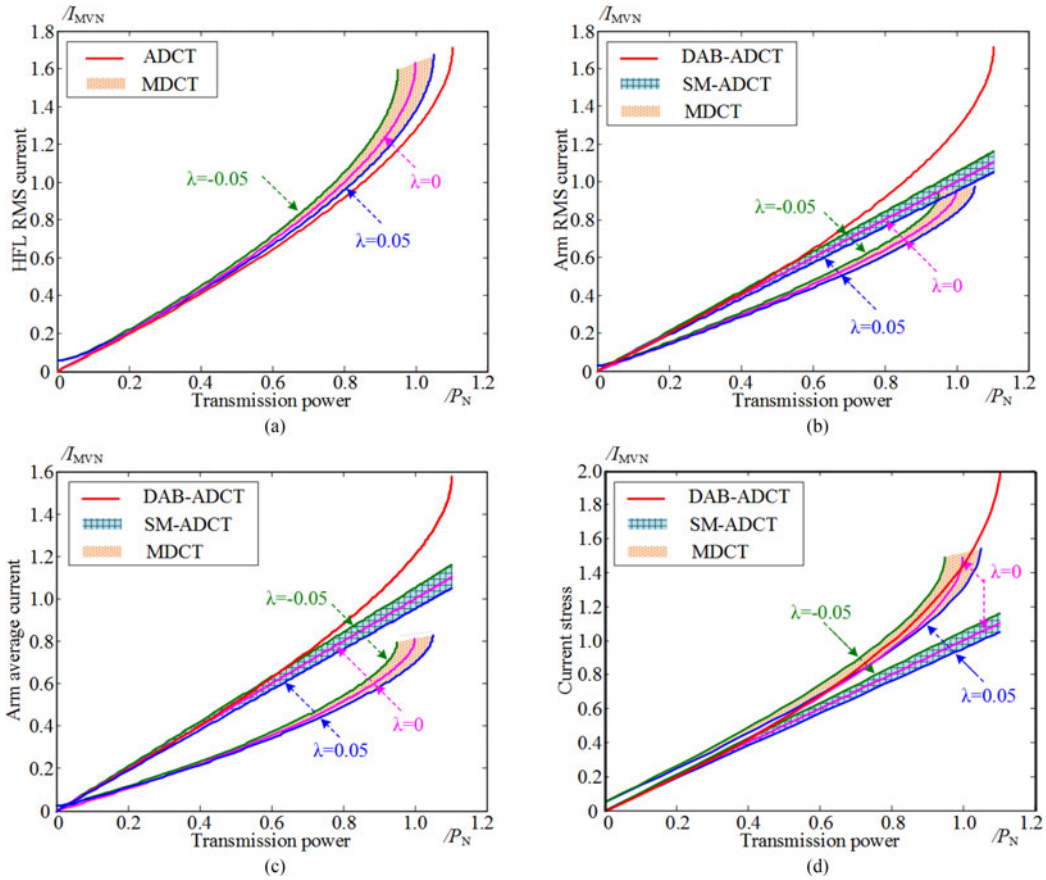

Fig. 6. Comparison of characteristic current for MDCT and ADCT in the MVDC side. (a) HFL RMS current. (b) Arm RMS current. (c) Arm average current. (d) Current stress.

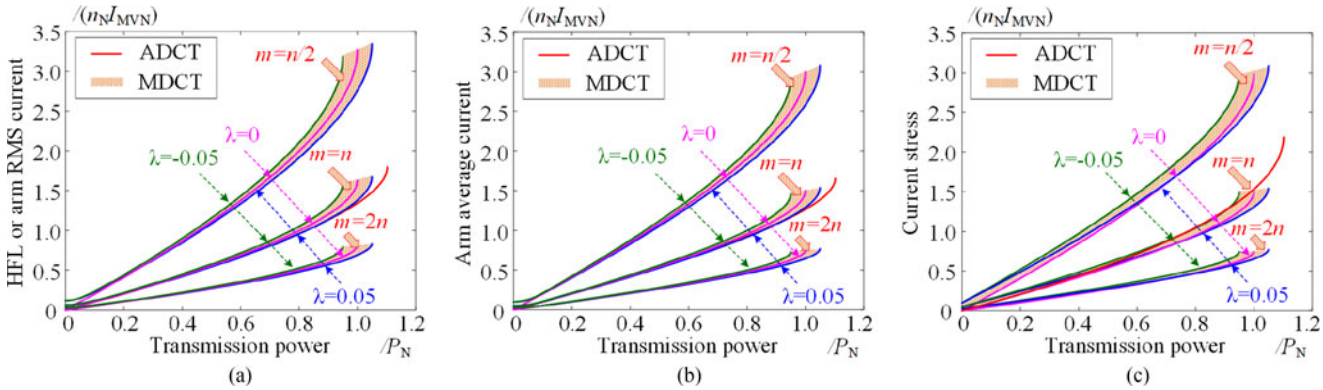

Fig. 7. Comparison of characteristic current for MDCT and ADCT in the LVDC side. (a) HFL or arm RMS current. (b) Arm average current. (c) Current stress.

ADCT. When $m = n$, all the characteristic currents of MDCT are almost the same with that of ADCT; however, because the HFL voltage of MDCT also changes with the fluctuation of the MVDC voltage and the HFL voltage of ADCT keep the constant, the characteristic currents of MDCT is an area but ADCT is a constant line. In Fig. 7, all the currents are normalized by $n_N I_{\mathrm{MVN}}$, where $n_N = V_{\mathrm{MVN}}/(nV_{\mathrm{LV}})$.

In practice, in order to satisfy the isolation of the MVDC system, the isolation voltage between the primary and the secondary sides of each transformer needs to be high, which increases the manufacturing difficulty and the volume of HF transformer greatly. Usually, reducing the number of HF transformer to a certain degree is welcome in practice. Therefore, considering that the number of H-bridges in ADCT is n, we usually do not select the number of H-bridges $m > n$ in MDCT.

VI. Switching Performance Comparison

A. Switching Performance Comparison in MVDC Side

Here, we just analyze the switching characterization when the power flows from MV side to LV side; the characterization with the different power flow can be analyzed similarly. In addition, because the turn-on loss of diode is very small in practice, it can be ignored in the analysis.

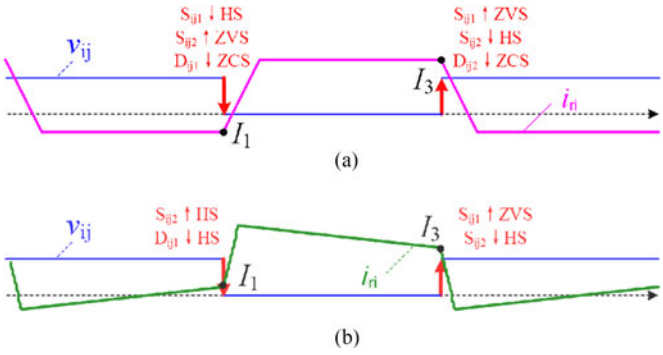

Fig. 8. Switching performance of MMC in MDCT. (a) Switching State 1. (b) Switching state 2.

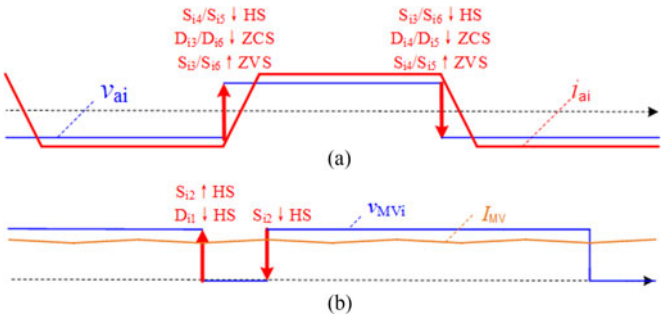

Fig. 9. Switching performance of ADCT in the MVDC side. (a) H-bridges in the MVDC side. (b) SM.

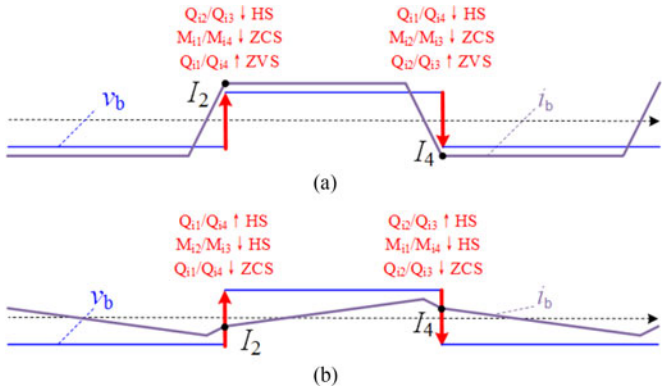

Fig. 10. Switching performance of H-bridges in MDCT. (a) Switching State 1. (b) Switching state 2.

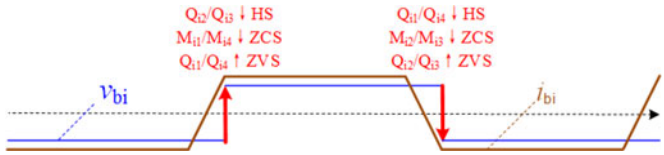

Fig. 11. Switching performance for H-bridges of ADCT in the LVDC side.

From the earlier analysis, there are different operation states for SMs in MDCT. Each operation state contains two typical switching behaviors. When MDCT operates with low voltage fluctuation, the arm current at switching time will have different polarity, as shown in Fig. 8(a). When $v_{ij} : 0 \rightarrow V_c$, the current is positive; when $v_{ij} : V_c \rightarrow 0$, the current is negative. Then, during one switching period, the soft switching behaviors are as follows: S_{aij1} turns on with zero voltage switching (ZVS), D_{ij2} turns off with zero current switching (ZCS), S_{ij2} turns on with ZVS, and D_{ij1} turns off with ZCS. The hard switching (HS) behaviors are as follows: S_{ij2} turns off, and S_{ij1} turns off. When the MDCT operates with high voltage fluctuation, the arm current at the switching time will have the same polarity, as shown in Fig. 8(b). When $v_{ij} : 0 \rightarrow V_c$, the current is positive; when $v_{ij} : V_c \rightarrow 0$, the current is still positive. Then, during one switching period, the soft switching behaviors are as follows: S_{ij1} turns on with ZVS. The HS behaviors are as follows: S_{ij2} turns on and turns off, and D_{ij1} turns off.

In ADCT, the DAB cell can always operate in matching state. No matter how the MVDC voltage fluctuates, all H-bridges in the MVDC side have the same switching behaviors, as shown in Fig. 9(a). All switches turn on with ZVS, and all diodes turn off with ZCS. The HS behaviors are just turn off for all the switches. The switching behaviors of SMs are shown in Fig. 9(b). All switching behaviors for the SMs are HS. During one switching period, there are turn on and turn off of switches and turn off of diodes. However, because the SMs in ADCT do not need to operate with HFL modulation, so the switching frequency can be small.

B. Switching Performance Comparison in the LVDC Side

Similar to the operation states for MMC in MDCT, the H-bridges in the LVDC side also contains two typical switching behaviors. As shown in Fig. 10(a), the MDCT operates with low voltage fluctuation or heavy load; the soft switching behaviors during one switching period are as follows: $Q_{i1} - Q_{i4}$ turn on with ZVS, $M_{i1} - M_{i4}$ turn off with ZCS. The HS behaviors are as follows: $Q_{i1} - Q_{i4}$ turn off. As shown in Fig. 10(b), the MDCT operates with high voltage fluctuation or load; the soft switching behaviors during one switching period are as follows: $Q_{i1} - Q_{i4}$ turn off with ZCS. The HS behaviors are as follows: $Q_{i1} - Q_{i4}$ turn on, and $M_{i1} - M_{i4}$ turn off.

Similar to the operation states for H-bridges of ADCT in the MVDC side, the H-bridges in LVDC also always operate in the matching state. No matter how the MVDC voltage fluctuates, all H-bridges have the same switching behaviors, as shown in Fig. 11. All switches turn on with ZVS, and all diodes turn off with ZCS. The HS behaviors are just turn off for all the switches.

According to the earlier analysis, the switching performance of MDCT will become worse when the MVDC voltage fluctuates, especially for the light-load situation. The switching performance of DABs in ADCT always remains the same, but the switching behaviors of SMs are added. However, in the MVDC side, because there exist $4n$ SMs for MMC in MDCT, so the number of switching behaviors of MDCT will be more than that of ADCT, even if SMs in ADCT are taken into account.

VII. Power Loss Comparison

In power loss analysis, to make a fair comparison, the MVDC and LVDC voltages and device rating voltage for MDCT and ADCT are the same, so if the number of SMs and DAB in ADCT is *n*, then the number of SMs for each arm is *n*. As for the number of H-bridges in MDCT, it can or cannot be *n*, which is defined with *m*. In this case, the number of switches in MDCT is $4*2*n+4*m=8n+4m$ and the number of switches in ADCT is $2*n+8*n=10n$, where *n* and *m* can be any positive integer according to the practical system.

A. Power Loss in the MVDC Side

In order to simplify the analysis, let us assume that the switch and the diode have the same voltage drop with the same current, which can be derived as

$$v_S = V_{S0} + R_S\left|i_S\right| \tag{11}$$

where v_S is the voltage drop, i_S is the current across the switches, V_{S0} is the threshold voltage, and R_S is the slope resistance. V_{S0} and R_S can be achieved from the datasheet of switches and diodes.

In MDCT, the current will always flow through one switch or diode for each SM. Then, *n* voltage drops are produced with the arm current for each arm. Similarly, in ADCT, each SM has one voltage drop and each H-bridge in DAB has two voltage drops. The instantaneous conduction power for MDCT and ADCT in MV side can be derived as

$$\begin{cases} p_{\mathrm{CON\_}M} = 4n\left(V_{S0}\left|i_{r\_M}\right| + R_S i_{r\_M}^2\right) \\ p_{\mathrm{CON\_}H1} = 2n\left(V_{S0}\left|i_{r\_H1}\right| + R_S i_{r\_H1}^2\right) \\ p_{\mathrm{CON\_SM}} = n\left(V_{S0}\left|i_{r\_\mathrm{SM}}\right| + R_S i_{r\_\mathrm{SM}}^2\right) \end{cases} \tag{12}$$

where $p_{\mathrm{CON\_}M}$, $p_{\mathrm{CON\_}H1}$, and $p_{\mathrm{CON\_SM}}$ are the instantaneous conduction power of MMC in MDCT, H-bridges, and SMs of ADCT in the MVDC side, respectively.

From (12), the average conduction loss during one switching period in the MVDC side can be derived as

$$\begin{cases} P_{\mathrm{CON\_}M} = \dfrac{1}{T}\displaystyle\int_0^T p_{\mathrm{CON\_}M}\,dt \\ = 4nV_{S0}\widehat{I}_{r\_M} + 4nR_S I_{r\_M}^2 \\ P_{\mathrm{CON\_}A1} = \dfrac{1}{T}\displaystyle\int_0^T \left(p_{\mathrm{CON\_}H1} + p_{\mathrm{CON\_SM}}\right)dt \\ = nV_{S0}\left(\widehat{I}_{r\_\mathrm{SM}} + 2\widehat{I}_{r\_H1}\right) + nR_S\left(I_{r\_\mathrm{SM}}^2 + 2I_{r\_H1}^2\right) \end{cases} \tag{13}$$

where $P_{\mathrm{CON\_}M}$ and $P_{\mathrm{CON\_}A1}$ are the average conduction power of MDCT and ADCT in the MVDC side, respectively.

From (13), the conduction loss can be divided into two parts, which are

$$\begin{cases} P_{\mathrm{CON\_}M1} = 4nV_{S0}\widehat{I}_{r\_M} \\ P_{\mathrm{CON\_}M2} = 4nR_S I_{r\_M}^2 \\ P_{\mathrm{CON\_}A11} = nV_{S0}\left(\widehat{I}_{r\_\mathrm{SM}} + 2\widehat{I}_{r\_H1}\right) \\ P_{\mathrm{CON\_}A12} = nR_S\left(I_{r\_\mathrm{SM}}^2 + 2I_{r\_H1}^2\right) \end{cases}. \tag{14}$$

In this case, the two parts of conduction loss in (14) can be normalized by P_{CON1} and P_{CON2}, respectively, where $P_{\mathrm{CON1}} = nV_{S0}I_{\mathrm{MVN}}$ and $P_{\mathrm{CON2}} = nR_S I_{\mathrm{MVN}}^2$. Then, the conduction loss of MDCT and ADCT in the MVDC side can be compared with two parts, as shown in Fig. 12(a) and (b). Although the current flows more switches in MDCT, because the arm current of MDCT is lower and the SMs are added in ADCT, the conduction loss of MDCT is lower than that of ADCT. However, the loss of the ADCT almost remains the same when the MVDC voltage changes, but the loss of the MDCT changes a lot.

From the analysis in Section VI, the HS behaviors of both DCTs involve not only turn off but also turn on. However, every turn-on behavior of the switch will be accompanied with a turn-off behavior of the diode. In order to simplify the analysis, let us assume that the turn-off loss of the switch is equivalent to the sum of the turn-on loss of the switch and the turn-off loss of the diode. Assuming that the normalized switching loss based on voltage and current is e_{SW}, from the analysis in Section VI, the switching loss of each SM during a switching period for MMC of MDCT in the MVDC side can be derived as

$$E_{\mathrm{SW\_}M} = \frac{e_{\mathrm{SW}}V_{\mathrm{MV}}\left(\left|I_1\right| + \left|I_3\right|\right)}{n} \tag{15}$$

where $E_{\mathrm{SW\_}M}$ is the switching loss of each SM during a switching period in MMC of MDCT.

For ADCT, because DAB always operates with matching state, ignoring current fluctuation in the MVDC side, the switching loss of each H-bridge and SM during a switching period in the MVDC side can be derived as

$$\begin{cases} E_{\mathrm{SW\_}H1} = \dfrac{4e_{\mathrm{SW}}(1+\lambda_{\max})V_{\mathrm{MVN}}I_{m\_H1}}{n} \\ E_{\mathrm{SW\_SM}} = \dfrac{2e_{\mathrm{SW}}(1+\lambda_{\max})V_{\mathrm{MVN}}I_{m\_\mathrm{SM}}}{n} \end{cases} \tag{16}$$

where $E_{\mathrm{SW\_}H1}$ and $E_{\mathrm{SW_SM}}$ are the switching losses of each H-bridge in the MVDC side and each SM during a switching period in MDCT, respectively.

From the switching characterization in Section VI, the average switching loss in the MVDC side can be derived as

$$\begin{cases} P_{\mathrm{SW\_}M} = 4nf_s E_{\mathrm{SW\_}M} \\ P_{\mathrm{SW\_}A1} = n\left(f_s E_{SW\_H1} + f_{\mathrm{SM}}E_{\mathrm{SW\_SM}}\right) \end{cases} \tag{17}$$

where $P_{\mathrm{SW\_}M}$ and $P_{\mathrm{SW\_}A1}$ are the average switching loss of MDCT and ADCT in the MVDC side, respectively.

From (15) to (17), the comparison of the switching loss for MDCT and ADCT in the MVDC side is shown in Fig. 12(c), where the switching loss is normalized by $P_{\mathrm{SW}} = f_s e_{\mathrm{SW}} P_N$. From Fig. 12(c), although the arm current of MMC in MDCT is lower than that of ADCT in the MVDC side, the peak current increases greatly when the MVDC voltage fluctuates, especially the number of switching behaviors of MDCT is more, the switching loss of MDCT will be higher than that of ADCT in the MVDC side, especially for light loads. In fact, for ADCT, although SMs are added, the switching frequency can be less than the HFL frequency. In this section, the switching frequency ratio for SM and DAB is $f_{\mathrm{SM}}/f_s = 1/2$.

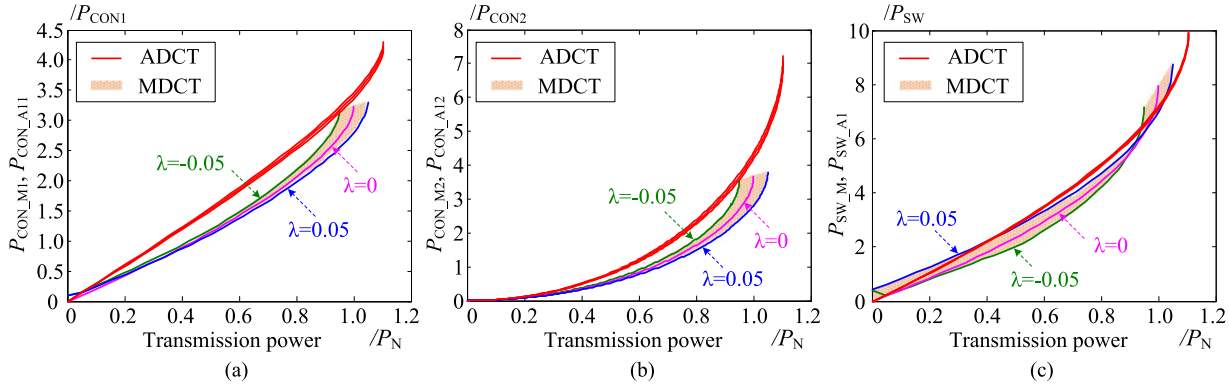

Fig. 12. Comparison of power loss for MDCT and ADCT in the MVDC side. (a) Part 1 of conduction loss. (b) Part 2 of conduction loss. (c) Switching loss.

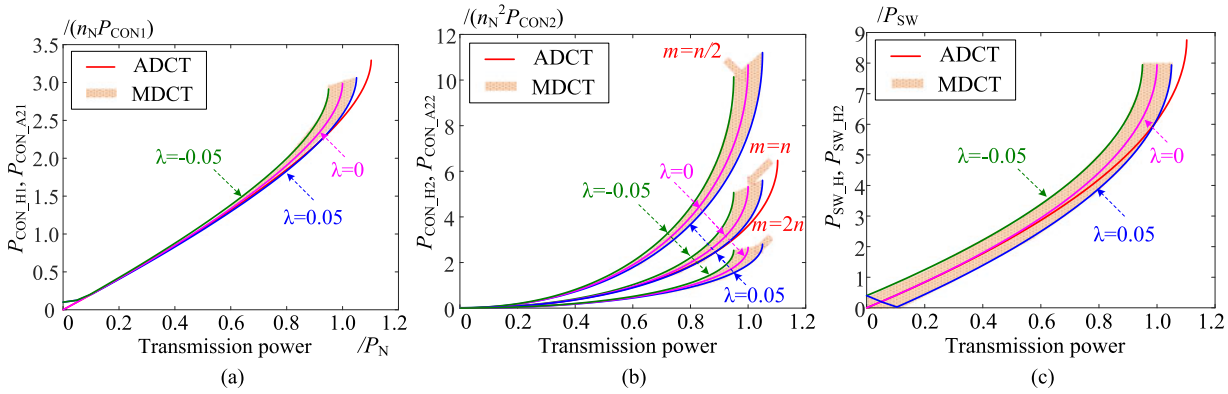

Fig. 13. Comparison of power loss for MDCT and ADCT in the LVDC side. (a) Part 1 of conduction loss. (b) Part 2 of conduction loss. (c) Switching loss.

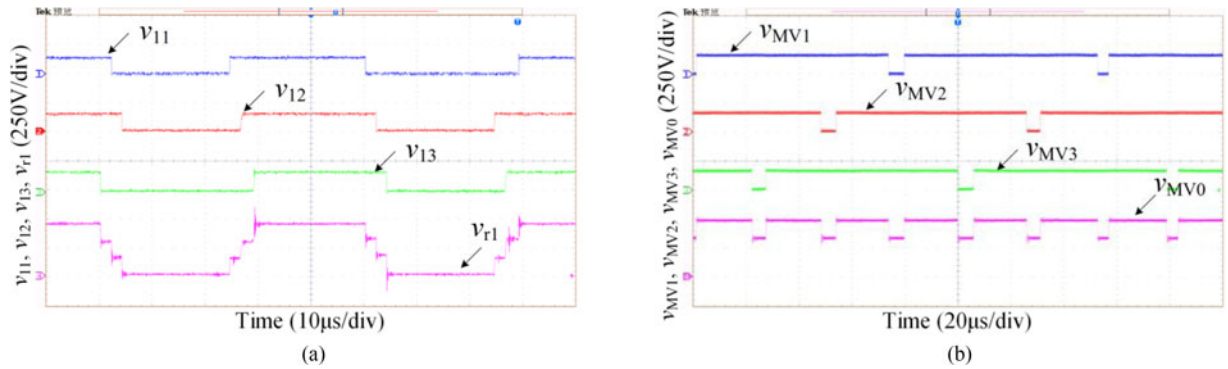

Fig. 14. Comparison of multilevel modulation for (a) MDCT and (b) ADCT.

B. Power Loss in the LVDC Side

Different with MMC in MDCT, there are just two voltage drops for the H-bridges in the LVDC side, and the number of H-bridges is m which can equal to n or not as analysis in Section V. Then, similar to the analysis in the MVDC side, the average conduction loss during one switching period in the LVDC side can be derived as

$$\begin{cases} P_{\mathrm{CON\_}H} = 2mV_{S0}\widehat{I}_{r\_H} + 2mR_S I_{r\_H}^2 \\ P_{\mathrm{CON\_}A2} = 2nV_{S0}\widehat{I}_{r\_H2} + 2nR_S I_{r\_H2}^2 \end{cases} \tag{18}$$

where $P_{\mathrm{CON\_}H}$ and $P_{\mathrm{CON\_}A2}$ are the average conduction power of MDCT and ADCT in the LVDC side, respectively.

Then, the conduction loss of MDCT and ADCT in the LVDC side can also be compared with two parts, as shown in Fig. 13(a) and (b), where the two parts are normalized by $n_N P_{\mathrm{CON1}}$ and $(n_N)^2 P_{\mathrm{CON2}}$. It can be seen that the conduction loss of ADCT is almost kept the same when the MVDC voltage changes. Part 1 of conduction loss related to average current does not change with the number of H-bridges in MDCT, but it changes with the fluctuation of the MVDC voltage, and the part 1 loss of MDCT is higher than that of ADCT because the average current

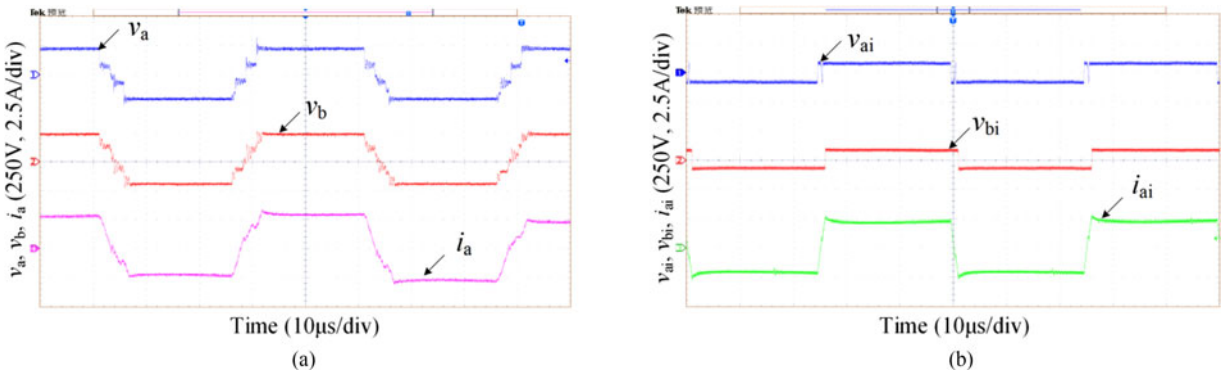

Fig. 15. Comparison of HFL operation for (a) MDCT and (b) ADCT.

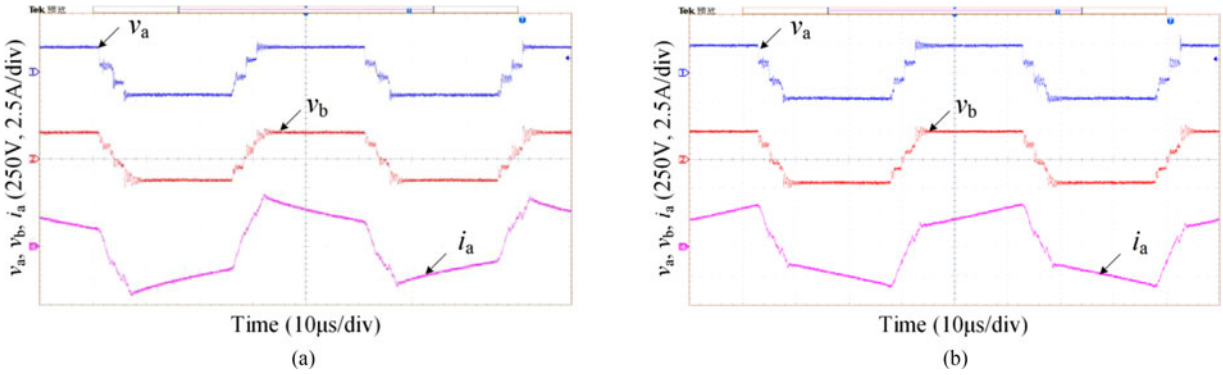

Fig. 16. Comparison of HFL operation for MDCT with MVDC voltage fluctuation. (a) $\lambda = -5\%$. (b) $\lambda = 5\%$.

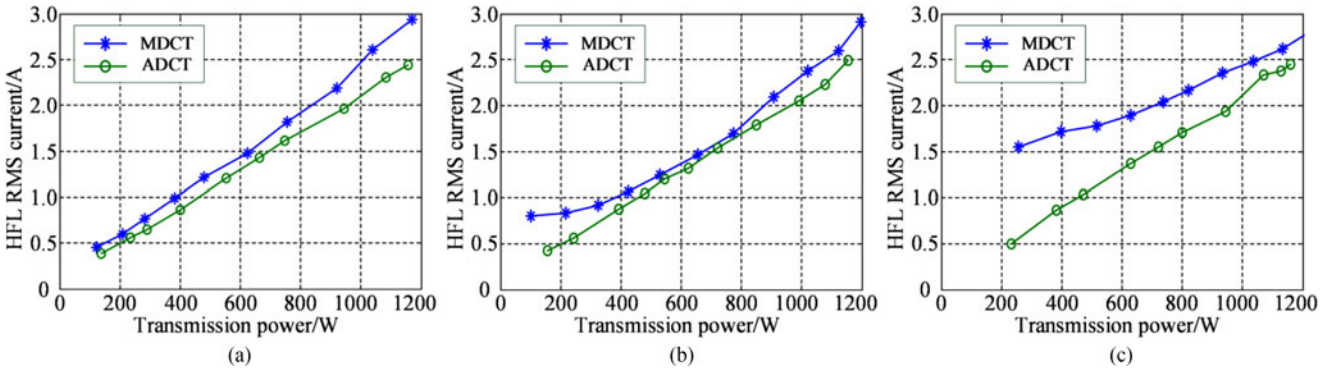

Fig. 17. Comparison of HFL currents for MDCT and ADCT with different voltage fluctuation. (a) $\lambda = -5\%$. (b) $\lambda = 0$. (c) $\lambda = 5\%$.

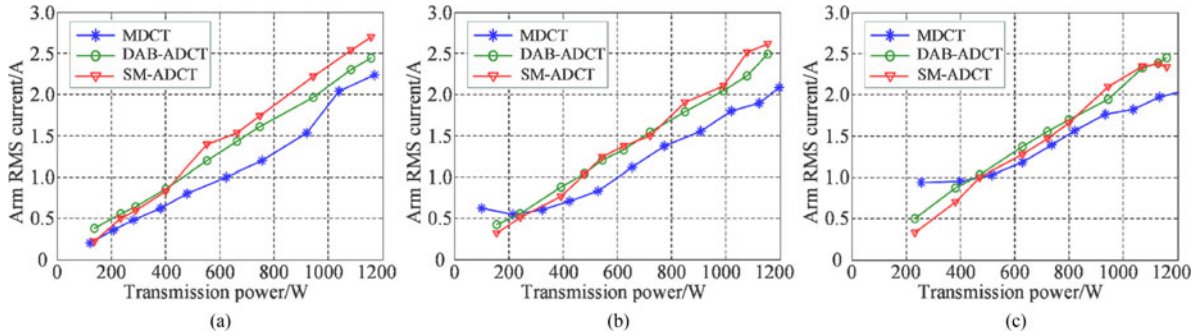

Fig. 18. Comparison of arm currents for MDCT and ADCT with different voltage fluctuation. (a) $\lambda = -5\%$. (b) $\lambda = 0$. (c) $\lambda = 5\%$.

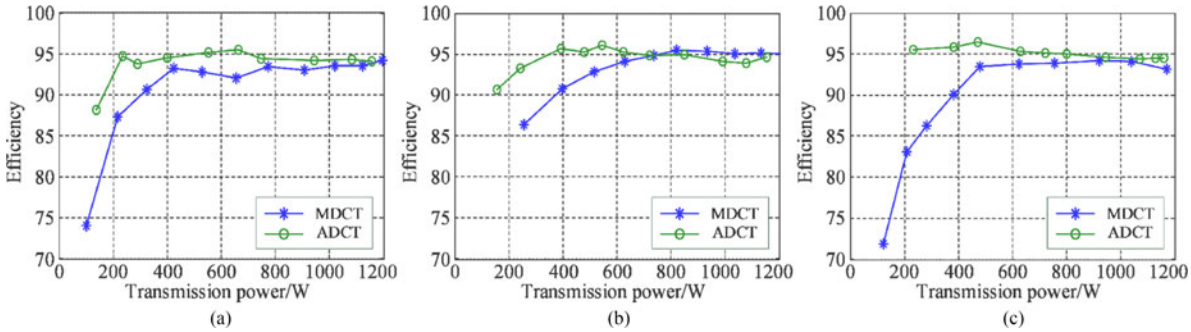

Fig. 19. Comparison of efficiencies for MDCT and ADCT with different voltage fluctuation. (a) $\lambda = -5\%$. (b) $\lambda = 0$. (c) $\lambda = 5\%$.

is higher. Part 2 of conduction loss related to RMS current in MDCT not only changes with the number of H-bridges but also changes with the fluctuation of the MVDC voltage. If we just consider $m \leq n$ in practice, the part 2 loss of MDCT is also higher than that of ADCT.

Similar to the analysis in the MVDC side, the average switching loss in the LVDC side can be derived as

$$\begin{cases} P_{\mathrm{SW\_}H} = mf_s E_{\mathrm{SW\_}H} = 2mf_s e_{\mathrm{SW}} V_{\mathrm{LV}} \left(|I_2| + |I_4|\right) \\ P_{\mathrm{SW\_}H2} = nf_s E_{\mathrm{SW\_}A2} = 4nf_s e_{\mathrm{SW}} V_{\mathrm{LV}} I_{m\_H2} \end{cases} \tag{19}$$

where $P_{\mathrm{SW\_}H}$ and $P_{\mathrm{SW\_}A2}$ are the average switching loss of MDCT and ADCT in the LVDC side, respectively.

The switching loss of MDCT and ADCT in the LVDC side is shown in Fig. 13(c), where the switching loss is also normalized by P_{SW}. It can be seen that the switching loss of ADCT is also kept the same when the MVDC voltage changes. The switching loss of MDCT in the LVDC side does not change with the number of H-bridges in MDCT but changes with the fluctuation of the MVDC voltage, and the loss is higher than that of ADCT during most of the ranges.

Notice that the analysis in this section mainly compares the power loss performance of ADCT and MDCT; we do not need to quantify absolute rationality and just need to make sure that the contrast to the law is reasonable, so some general assumptions are made in this section to simplify analysis.

VIII. Experimental Verification

To verify the theoretical earlier analysis, the small-scale MDCT and ADCT prototypes with 1 kW are built, and the parameters are as follow: MVDC- and LVDC-rated voltages are $V_{\mathrm{MV}} = 450\,\mathrm{V}$ and $V_{\mathrm{LV}} = 150\,\mathrm{V}$, respectively; the number of SMs and full bridges is $n = m = 3$; the transformer ratio is $n_T = 1:1$; the arm inductance is 30 μH; the leakage inductance of each transformer is 40 μH; the dc capacitors are $C_{ij} = 450\,\mu\mathrm{F}$ and $C_i = 450\,\mu\mathrm{F}$; and the switching frequency is $f_s = 20\,\mathrm{kHz}$.

Fig. 14 shows the comparison of multilevel modulation of MDCT and ADCT. In MDCT, the duty cycle for each SM is 50%. However, to decrease *dv*/*dt* in HFL, there is a small phase shift between the output voltages of each SM, so the HFL voltage is a multilevel trapezoidal wave in practice. In addition, from Section III, the alternate modulation for SM is employed to keep the balance of the dc capacitor, but no matter how it alternates, both the total high and low levels are 50% during one period. In ADCT, the multilevel modulation is in DCL, but the output of each SM is not a square wave with 50% duty ratio, which changes with the MVDC voltage. In order to decrease the current ripple, there is a $2\pi/3$ phase-shift angle between neighboring SMs.

Fig. 15 shows the comparison of HFL waveforms of MDCT and ADCT. Both MDCT and ADCT employ dual-active phase-shift control method. However, the HFL peak voltage of MDCT is almost three times that of ADCT, which is higher than that of ADCT. With the same transmission power, the HFL peak current of MDCT is higher than that of ADCT. In Fig. 16, $V_{\mathrm{MV}} = 450\,\mathrm{V}$ and $V_{\mathrm{LV}} = 150\,\mathrm{V}$, and both DCTs operate in matching state.

If voltage fluctuation in MVDC distribution grid is considered, the HFL waveforms of MDCT are shown in Fig. 16. With the voltage fluctuation of MVDC grid, the MDCT changes from matching state to mismatching state, and the current stress increases greatly. In addition, for ADCT, no matter how the MVDC voltage changes, the HFL current in ADCT remains the same with Fig. 15(b), which is lower than that of MDCT with the same transmission.

Fig. 17 shows the comparison of HFL currents of MDCT and ADCT with different voltage fluctuation. It can be seen that the HFL current of MDCT changes with the change of the MVDC voltage but the HFL current of ADCT almost keep the same. No matter how the MVDC voltage fluctuates, the MDCT has higher HFL current than that of ADCT with the same transmission power.

Fig. 18 shows the comparison of arm currents of MDCT and ADCT with different voltage fluctuation. It can be seen that the MDCT has lower arm current than ADCT with the same transmission power during most of the range. With the increase in the MVDC voltage, the current of SMs in ADCT decreases.

Fig. 19 shows the comparison of efficiencies of MDCT and ADCT with different voltage fluctuations. With the increase in the MVDC voltage, the average efficiency of ADCT increases. However, for MDCT, the conduction and switching losses have different regulation with the change of the voltage, and thus, the change is different. The matching state of MDCT has the highest efficiency. During matching state, the efficiency of MDCT may be higher than that of ADCT in some situations, but the ADCT has higher efficiency during most of the range.

IX. Conclusion

The performances of MDCT and ADCT are compared comprehensively for MVDC application in this paper. From the theoretical and experimental results, both MDCT and ADCT have fault treatment ability. However, the installation and commissioning of ADCT are more flexible and simpler. MDCT needs more switches and HF inductors than ADCT in the MVDC side, but the number of HF transformer can be reduced, which is welcome in practice. Compared with MDCT, ADCT has higher power transfer ability and lower circulating power and has lower HFL voltage and RMS current and peak values. However, the arm RMS and average currents of MDCT are lower than those of ADCT. The switching performance of MDCT becomes bad when the MVDC voltage fluctuates, but the switching behaviors of half bridges are added to ADCT. The loss of ADCT almost remains the same when the MVDC voltage fluctuates, but the loss of MDCT changes a lot.

References

[1] M. Davari and Y. A. R. I. Mohamed, "Dynamics and robust control of a grid-connected VSC in multiterminal dc grids considering the instantaneous power of dc- and ac-side filters and dc grid uncertainty," *IEEE Trans. Power Electron.*, vol. 31, no. 3, pp. 1942–1958, Mar. 2016.

[2] M. T. Daniel, H. S. Krishnamoorthy, and P. N. Enjeti, "An improved offshore wind turbine to MVDC grid interface using high frequency resonant isolation and input power factor control," in *Proc. IEEE Power Energy Conf. Illinois*, 2015, pp. 1–8.

[3] G. P. Adam, I. A. Abdelsalam, K. H. Ahmed, and B. W. Williams, "Hybrid multilevel converter with cascaded H-bridge cells for HVDC applications: operating principle and scalability," *IEEE Trans. Power Electron.*, vol. 30, no. 1, pp. 65–77, Jan. 2015.

[4] N. Flourentzou, V. G. Agelidis, and G. D. Demetriades, "VSC-based HVDC power transmission systems: An overview," *IEEE Trans. Power Electron.*, vol. 24, no. 3, pp. 592–602, Mar. 2009.

[5] V. Nayanar, N. Kumaresan, and N. A. Gounden, "A single-sensor-based MPPT controller for wind-driven induction generators sypplying dc microgrid," *IEEE Trans. Power Electron.*, vol. 31, no. 2, pp. 1161–1172, Feb. 2016.

[6] M. J. Carrizosa, A. Benchaib, P. Alou, and G. Damm, "DC transformer for dc/dc connection in HVDC network," in *Proc. 15th Eur. Power Electron. Appl.*, 2013, pp. 1–10.

[7] A. Mohammadpour, L. Parsa, M. H. Todorovic, R. Lai, R. Datta, and L. Garces, "Series-input parallel-output modular-phase dc–dc converter with soft switching and high frequency isolation," *IEEE Trans. Power Electron.*, vol. 31, no. 1, pp. 111–1119, Jan. 2016.

[8] N. Denniston, A. M. Massoud, S. Ahmed, and P. N. Enjeti, "Multiple-module high-gain high-voltage dc–dc transformers for offshore wind energy systems," *IEEE Trans. Ind. Electron.*, vol. 58, no. 5, pp. 1877–1886, May 2011.

[9] R. C. Youngquist, C. M. Ihlefeld, and S. O. Starr, "A dc transformer," *IEEE Trans. Power Electron.*, vol. 29, no. 1, pp. 42–44, Jan. 2014.

[10] Z. Zhang, Z. Ouyang, O. C. Thomesen, and M. A. E. Andersen, "Analysis and design of a bidirectional isolated dc–dc converter for fuel cells and supercapacitors hybrid system," *IEEE Trans. Power Electron.*, vol. 27, no. 2, pp. 848–859, Feb. 2012.

[11] B. Zhao, Q. Song, W. Liu, and Y. Sun, "Overview of dual-active-bridge isolated bidirectional dc–dc converter for high-frequency-link power- conversion system," *IEEE Trans. Power Electron.*, vol. 29, no. 8, pp. 4091–4106, Aug. 2014.

[12] Y. Xie, J. Sun, and J. S. Freudenberg, "Power flow characterization of a bidirectional galvanically isolated high-power dc–dc converter over a wide operating range," *IEEE Trans. Power Electron.*, vol. 25, no. 1, pp. 54–66, Jan. 2010.

[13] D. Costinett, D. Maksimovic, and R. Zane, "Design and control for high efficiency in high step-down dual active bridge converters operating at high switching frequency," *IEEE Trans. Power Electron.*, vol. 28, no. 8, pp. 3931–3940, Aug. 2013.

[14] S. Inoue and H. Akagi, "A bidirectional isolated dc–dc converter as a core circuit of the next-generation medium-voltage power conversion system," *IEEE Trans. Power Electron.*, vol. 22, no. 2, pp. 535–542, Mar. 2007.

[15] N. H. Baars, J. Everts, C. G. E. Wijnands, and E. A. Lomonova, "Performance evaluation of a three-phase dual active bridge dc–dc converter with different transformer winding configurations," *IEEE Trans. Power Electron.*, vol. 31, no. 10, pp. 6814–6823, Oct. 2016.

[16] A. F. Martinez, S. B. Monge, J. N. Apruzzese, and J. Bordonau, "Operating principle and performance optimization of a three-level NPC dual-active-bridge dc–dc converter," *IEEE Trans. Ind. Electron.*, vol. 63, no. 2, pp.678–690, Feb. 2016.

[17] G. E. Sfakianakis, J. Everts, H. Huisman, and E. A. Lomonova, "ZVS modulation strategy for a 3-5 level bidirectional dual active bridge dc–dc converter," in *Proc. 11th Int. Conf. Ecol. Veh. Renewable Energies*, 2016, pp. 1–9.

[18] G. E. Sfakianakis, J. Everts, H. Huisman, and E. A. Lomonova, "Comparative evaluation of bidirectional dual active bridge dc–dc converter variants," in *Proc. IEEE Veh. Power Propulsion Conf.*, 2016, pp. 1–6.

[19] D. Aggeler, J. Biela, and J. W. Kolar, "A compact, high voltage 25 kW, 50 kHz dc–dc converter based on SiC JFETs," in *Proc. 23th IEEE Annu. Appl. Power Electron. Conf. Expo.*, 2008, pp. 801–807.

[20] P. Zumel *et al.*, "Modular dual-active-bridge converter architecture," *IEEE Trans. Ind. Appl.*, vol. 52, no. 3, pp. 2444–2455, May/Jun. 2016.

[21] X. She *et al.*, "Review of solid state transformer in the distribution system: From components to field application," in *Proc. IEEE Energy Convers. Congr. Expo.*, 2012, pp. 4077–4084.

[22] M. Sato *et al.*, "High efficiency design for ISOP converter system with dual active bridge dc–dc converter," in *Proc. IEEE Appl. Power Electron. Conf. Expo.*, 2016, pp. 2465–2472.

[23] T. Todorcevic, R. Kessel, P. Bauer, and J. A. Ferreira, "A modulation strategy for wide voltage output in DAB-based dc–dc modular multilevel converter for DEAP wave energy conversion," *IEEE J. Emerg. Sel. Topics Power Electron.*, vol. 3, no. 4, pp. 1171–1181, Dec. 2015.

[24] B. Zhao, Q. Song, J. Li, Y. Wang, and W. Liu, "High-frequency-link modulation methodology of dc–dc transformer based on modular multilevel converter for HVDC application: Comprehensive analysis and experimental verification," *IEEE Trans. Power Electron.*, vol. 32, no. 5, pp. 3413–3424, May 2017.

[25] S. P. Engel, M. Stieneker, N. Soltau, S. Rabiee, H. Stagge, and R. W. D. Doncker, "Comparison of the modular multilevel dc converter and the dual-active bridge converter for power conversion in HVDC and MVDC grids," *IEEE Trans. Power Electron.*, vol. 30, no. 1, pp. 124–137, Jan. 2015.

[26] K. Filsoof and P. W. Lehn, "A bidirectional modular multilevel dc–dc converter of triangular structure," *IEEE Trans. Power Electron.*, vol. 30, no. 1, pp. 54–64, Jan. 2015.

[27] S. Kenzelmann, A. Rufer, D. Dujic, F. Canales, and Y. R. de Novaes, "Isolated dc/dc structure based on modular multilevel converter," *IEEE Trans. Power Electron.*, vol. 30, no. 1, pp. 89–98, Jan. 2015.

[28] T. Luth, M. M. C. Merlin, T. C. Green, F. Hassan, and C. D. Barker, "High-frequency operation of a dc/ac/dc system for HVDC applications," *IEEE Trans. Power Electron.*, vol. 29, no. 8, pp. 4107–4115, Aug. 2014.

[29] B. Zhao, Q. Song, J. Li, Y. Wang, and W. Liu, "Modular multilevel high-frequency-link dc transformer based on dual-active phase-shift principle for medium-voltage dc power distribution application," *IEEE Trans. Power Electron.*, vol. 32, no. 3, p. 99, Mar. 2017.

[30] B. Zhao, Q. Song, J. Li, W. Liu, G. Liu, and Y. Zhao, "High-frequency-link dc transformer based on switched capacitor for medium-voltage dc power distribution application," *IEEE Trans. Power Electron.*, vol. 31, no. 7, pp. 4766–4777, Jul. 2016.

Biao Zhao (S'11–M'14) was born in Hubei, China, in 1987. He received the B.S. degree from the Department of Electrical Engineering, Dalian University of Technology, Dalian, China, in 2009, and the Ph.D. degree form the Department of Electrical Engineering, Tsinghua University, Beijing, China, in 2014.

His current research interests include high power dc–dc converter, power electronic transformer, and flexible dc transmission and distribution system.

Dr. Zhao is a member of the IEEE Power Electronics Society, the Industrial Electronics Society, and the Chinese Society for Electrical Engineering.

Qiang Song (M'14) was born in Changchun, China, in 1975. He received the B.S. and Ph.D. degrees from the Department of Electrical Engineering, Tsinghua University, Beijing, China, in 1998 and 2003, respectively.

He is currently an Associate Professor in the Department of Electrical Engineering, Tsinghua University. His current research interests include high power electronic interfaces for utility system, flexible ac transmission system, and motor drives.

Jianguo Li was born in Hebei, China in 1975. He received the B.S. degree from the Department of Electrical Engineering, North China Electric Power University, Baoding, China, in 1997, the M.S. degree from the Department of Electrical Engineering, Tsinghua University, Beijing, China, in 2005, and the Ph.D. degree from the Department of Electrical Engineering, North China Electric Power University, Beijing, China, in 2017.

His current research interests include bidirectional dc–dc converter, high-frequency-link power conversion system, and flexible dc transmission and distribution system.

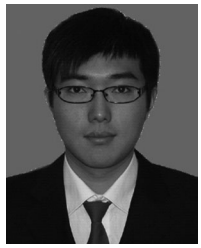

Xiaopeng Xu was born in Liaoning, China, in 1987. He received the B.S. degree from the Department of Electrical Engineering, Dalian University of Technology, Dalian, China, in 2009, and the M.S. degree from the Department of Electrical Engineering, North China Electric Power University, Baoding, China, in 2016.

He is currently a Power Dispatcher in Liaoning Electric Power Company Limited, Liaoning. His current research interests include power system dispatching technology, flexible transmission, and distribution system.

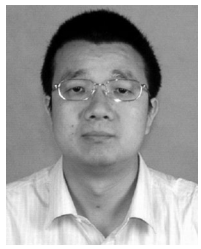

Wenhua Liu was born in Hunan, China, in 1968. He received the B.S., M.S., and Ph.D. degrees from the Department of Electrical Engineering, Tsinghua University, Beijing, China, in 1988, 1993, and 1996, respectively.

He is currently a Professor in the Department of Electrical Engineering, Tsinghua University. His current research interests include high power electronic and flexible ac transmission system.